Journal of Membrane Science 675 (2023) 121540

Contents lists available at ScienceDirect

Journal of Membrane Science

journal homepage: www.elsevier.com/locate/memsci

Highly porous ultrathin polyamide membranes for fast separation of small molecules from organic solvents

Siyan Wang, Zhenggong Wang, Shouwen Zhu, Shuqi Liu, Feng Zhang **, Jian Jin *

College of Chemistry, Chemical Engineering and Materials Science, Collaborative Innovation Center of Suzhou Nano Science and Technology, Suzhou Key Laboratory of Macromolecular Design and Precision Synthesis, Jiangsu Key Laboratory of Advanced Negative Carbon Technologies, Soochow University, Suzhou, 215123, China

ARTICLE INFO

Keywords:
Organic solvent nanofiltration
Molecule separation
Adamantane structure
High permeance
Solvent resistance

ABSTRACT

Membranes with permselective performance as well as high stability in harsh solvents are urgently desired for energy-efficient precise chemical separations. In this work, we utilize an adamantane diamine as a molecular building block to fabricate thin-film composite polyamide membranes for high-performance organic solvent nanofiltration (OSN). The bulky, cage-like adamantane structure acts as a molecular-level steric hindrance unit to inhibit polymer chain packing which generating interconnected micropores within the interfacially polymerized polyamide layer. This translates into high membrane methanol permeance of 20.6 L m^{-2} h^{-1} bar^{-1} and 94.7% retention to organic dye molecules with molecular weight down to 327 g mol^{-1}. Furthermore, the membrane demonstrates high stability in different organic solvents taking advantage of the crosslinked rigid structure, which shows constant solute retention throughout a 180 h continuous filtration experiment with a DMF solution containing methyl orange as feed solution. Employing rigid and bulky molecular features in selective layer is thus demonstrated to significantly promote the polyamide membrane permeability and solvent resistance without compromising the overall selectivity.

1. Introduction

Membrane technology has been broadly utilized in purification and separation processes due to its low energy consumption and small carbon footprints comparing to traditional chemical engineering processes involving distillation, adsorption, or extraction. Among various membrane-based technologies, organic solvent nanofiltration (OSN) is a burgeoning technique for molecular separation in organic solvents with molecular weight cut-off (MWCO) of 200–1000 Da [1–4]. Due to the harsh working conditions for OSN, the membranes must be robust enough in organic solvents, simultaneously possessing high permeance and selectivity in a wide range of organic solvents with different polarities. However, hampered by the trade-off between membrane permeability and selectivity, realizing fast and fine molecular separation is still a great challenge for OSN.

Strategies for making OSN membranes with enhanced permeance usually involve reducing the membrane thickness and increasing the intrinsic permeability of the membrane material [5,6]. Emerging crystalline materials like metal organic frameworks (MOFs) and covalent organic frameworks (COFs) with three-dimensional crosslinked structure and defined interconnected pore structures could be ideal materials for highly permselective OSN membranes [7–12]. But fabrication of defect-free membranes, especially ultrathin membranes using these crystalline materials remains a technical challenge [8,9,11,13]. Interfacial polymerization has been widely used for the fabrication of highly crosslinked and ultrathin composite membrane [14,15], and the thin film composite (TFC) membranes possess good solvent resistance and solute rejection performance. However, the TFC membranes fabricated using traditional monomers fail to achieve high solvent permeance due to lack of free volumes in the polymer network. Using new monomeric building blocks to improve the performance of the membrane is thus intensively investigated [16–19]. Polymers of intrinsic microporosity (PIMs) are a class of polymers with microporous structure formed by inefficient stacking of molecular segments, which is well known for high specific surface area and ultra-high permeability [20,21]. Inspired by the molecular structure design of PIMs, crosslinked polymer membranes with enhanced microporosity were fabricated using contorted monomers [22–24]. For example, the polyarylate membranes fabricated by spirostructured 5,5′,6,6′-tetrahydroxy-3,3,3′,3′-tetramethylspirobisindane and cardo-structured 9,9-bis(4-hydroxyphenyl)fluorene as

* Corresponding author.
** Corresponding author.
E-mail addresses: fzhang2018@suda.edu.cn (F. Zhang), jjin@suda.edu.cn (J. Jin).

https://doi.org/10.1016/j.memsci.2023.121540
Received 14 December 2022; Received in revised form 24 February 2023; Accepted 27 February 2023
Available online 1 March 2023

molecular building blocks demonstrated significantly improved organic solvent permeability [22]. Although incorporation of contorted structure can increase the permeability of the selective layer, the selectivity is usually sacrificed due to the generated micropores. Besides, the way of forming micropores by contorted structure is a physical relaxation phenomenon [25,26]. The interchain distance tends to be enlarged under pressure or challenged by aggressive organic solvents, resulting in undermined membrane selectivity in OSN applications. From this point of view, engineering design of high performance OSN membranes should consider both high microporosity and robust structure.

Herein, we propose an approach that using a rigid and bulky adamantane structure as the main building block of the selective layer to increase the free-volume and robustness of the membrane. Adamantane is a diamond-like cage structure aliphatic hydrocarbon composed of three fused cyclohexane rings arranged in chair conformation, which results in a bulky structure with 1.7 times the molecular volume of a phenyl group [27,28]. The bulky adamantyl moieties within polymer networks tend to disrupt chains stacking and improve membrane microporosity [29–31]. Notably, the highly symmetrical structure and spherical molecular morphology lead to a rigid cage-like chair configuration, endowing the adamantane structure with low strain energy and no angular or ring tension. Several studies have found that incorporating rigid adamantane segments helps to prevent polymer chain swelling and results in modified polymers with improved solvent tolerance in harsh conditions [27,32,33]. In this work, a highly permeable and selective thin-film composite OSN membrane was fabricated via interfacial polymerization using adamantane-1,3-diamine (AdDA) as the aqueous phase monomer. The bulky cage-like adamantane groups function as molecular-level steric hindrance unit to prevent the close packing of polymers chain, thus generate interconnected micropores within polymer networks. The TFC membrane prepared by AdDA shows methanol permeance of about 20.6 L m^{-2} h^{-1} bar^{-1} and MWCO down to 320 Da, which is superior to that of most reported OSN membranes reported in literature. In addition, the rigid AdDA-based polyamide network is mechanically robust and performs good resistance toward organic solvents, including N, N-dimethylformamide (DMF) during over 180 h continuous filtration.

2. Experimental section

2.1. Materials

Polyimide polymer (P84) was purchased from HP Polymer GmbH (Austria) and dried under vacuum at 120 °C for 24 h. Adamantane-1,3-diamine (AdDA, 98.0%), trimesoyl chloride (TMC, 99.0%), 1,6-hexanediamine (HDA, 98.0%), and m-phenylenediamine (MPD, 98.0%) were purchased from TCI. Anhydrous piperazine (PIP, 99.0%), chrysoidine G (CSG, 248.7 g mol^{-1}, 97.0%), methyl orange (MO, 327.3 g mol^{-1}, 96.0%), rhodamine B (Rh B, 479.0 g mol^{-1}, 95.0%), acid fuchsin (AF, 585.5 g mol^{-1}, 97.0%), congo red (CR, 696.7 g mol^{-1}, 98.0%), Coomassie brilliant blue G250 (CBB, 854.0 g mol^{-1}, 98.0%), and rose bengal (RB,1017.6 g mol^{-1}, 95.0%) were obtained from Aladdin Chemistry Co., Ltd. (Shanghai, China). Other chemicals, including methanol (MeOH, 99.5%), ethanol (EtOH, 99.7%), isopropyl alcohol (IPA, 99.5%), toluene (99.5%), *n*-hexane (97.0%), tetrahydrofuran (THF, 99.5%), N, N-dimethylformamide (DMF, 99.5%), acetone (99.5%), acetonitrile (99.0%) and sodium hydroxide (96.0%) were all purchased from Sinopharm Chemical Reagent Co., Ltd. (Shanghai, China). All chemicals and reagents were of analytical grade and used as received without further purification. Deionized (DI) water (Resistance = 18.2 MΩ) used in all experiments was filtered through a Millipore Milli-Q water purification system.

2.2. Preparation of crosslinked P84 (XP84) ultrafiltration support

P84 ultrafiltration supports were prepared using nonsolvent-induced phase inversion (NIPS) method. To prepare the P84 casting solution, 20 wt% P84 powder was added to DMF and the solution was stirred overnight in a sealed container at room temperature. The obtained homogenous solution was de-gased naturally for 24 h. The P84 solution was cast on polypropylene nonwoven support at a thickness of 200 μm at constant temperature (25 °C) and humidity (60%) and then phase inversion in water to obtain P84 ultrafiltration membranes. Then, the prepared P84 ultrafiltration membranes were transferred into IPA exchange bath for an additional day to further remove residual solvents. Crosslinking of P84 was conducted using HDA crosslinker [34]. The resulting crosslinked P84 membranes were named as XP84 and stored in deionized water at 5 °C.

2.3. Preparation of thin film composite membranes

The AdDA based polyamide (PA-AdDA) thin film composite (TFC) membranes were prepared directly on XP84 supports. The PA-AdDA TFC membranes were prepared by interfacial polymerization of AdDA in water and TMC in *n*-hexane using the method described in previous work [35,36]. XP84 support was placed on a glass plate and 2 mL aqueous solution containing AdDA with certain concentrations (ranging from 0.2 to 0.8 wt%) was poured onto the support and stood for 2 min. The membrane was then lifted upright to remove all the excess AdDA solution until no water spots was observed. The membrane was sealed again and wetted by 2 mL *n*-hexane solution containing 0.32 wt% (w/v) TMC for 10–60 s. After reaction, the membrane was washed by *n*-hexane to remove excess TMC and cured in oven at 60 °C for 10 min to complete crosslinking. Polyamide oligomer fragments inside membrane were removed by immersing membranes in DMF for 8 h. The corresponding stoichiometry ratio between AdDA and TMC are calculated and shown in Table S1. The resulting membranes were submersed in deionized water and stored in a laboratory refrigerator at 5 °C. All preparation experiments were conducted at 25 °C and relative humidity of about 50%. The TFC membrane using MPD as monomer in aqueous solution was fabricated in similar process. The concentration of the MPD in water and the TMC in *n*-hexane were 0.4 wt% and 0.32 wt%, respectively, and the reaction time was 10 s. The as-prepared membrane was named as PA-MPD TFC membrane.

2.4. Preparation of free-standing polyamide nanofilms

The free-standing polyamide nanofilms were prepared by interfacial polymerization of diamines in aqueous solution (0.4 wt%) and TMC in *n*-hexane (0.32 wt%) with the reaction time of 10s. Three diamines including PIP, MPD and AdDA were used to fabricate polyamide nanofilms, the as-prepared nanofilms were named as PA-PIP, PA-MPD and PA-AdDA nanofilm, respectively.

2.5. Characterizations

Gas adsorption experiments were conducted on Quantachrome Instrument at 77 k (N_2 adsorption) or 273 K (CO_2 adsorption) using free-standing nanofilms. Bruker D8 Advance X-ray diffractometer with Cu Kα radiation source possessing a wavelength of 1.54 Å was used to study X-ray diffraction (XRD) patterns with scanning speed of 0.02°/s in a range from 10° to 50°. The morphologies of membranes were characterized by field emission scanning electron microscope (FE-SEM; Regulus 8230, Hitachi, Japan) and atomic force microscopy (AFM; Dimension Icon, Brucker, USA). The cross-sectional images were observed by Transmission electron microscopy (TEM; TecnaiG2F20, FEI, USA). The membranes were first embedded in epoxy resin, then the thin sections with approximately 100 nm were cut using a frozen ultrathin slicer and collected on copper grids for TEM analysis. Attenuated total reflectance Fourier transform infrared spectrometer (ATR-FTIR; Nicolet 6700, USA) and X-ray photoelectron spectroscopy (XPS; EXCALAB 250 Xi, Thermo Scientific, USA) were used to determine the chemical bonding and

elemental compositions of membrane surface. Thermogravimetric analysis (TGA) was performed in N_2 atmosphere using TG/DTA 6200, in the temperature range between 40 and 800 °C with a heating rate of 10 °C/min. Differential scanning calorimetry (DSC) was carried out using TA instrument (DSC Q2000) at a heating rate of 5 °C/min from 25 to 125 °C in N_2 atmosphere. Thermal history was erased before actual measurement by heating up to 125 °C. Solid surface zeta potential was investigated by using a SurPASS electrokinetic analyzer. Static contact angle was tested through a Data-Physics OCA20 with 1 μl organic solvent droplet. UV–vis spectrometer (UV-2600, Japan) was employed to determine dye concentration of solutions.

2.6. OSN performance evaluation

Separation performance of membrane was evaluated according to permeance, dye rejection and long-term stability in organic solvents and was carried out on a dead-end filtration system with effective membrane area of 3.14 cm^2. Solvents (MeOH, EtOH, IPA, toluene, acetonitrile, acetone, DMF and THF) and dye solutions (CSG, MO, RhB, AF, CR, BBG, BR) were employed to evaluate the membrane performance. Before measurements, the selected solvent was filtered through the membranes under 10 bar for 6 h to compact the membrane. Permeate samples for flux were collected after steady permeate flux was achieved.

The solvent flux (J, L m^{-2} h^{-1}) was determined using equation (1):

$$J = \Delta w / \rho A \Delta t \tag{1}$$

where Δw is the weight of the collected permeate during the filtration time Δt, ρ is the density of the collected sample, and A is the effective membrane area.

Permeance (P, L m^{-2} h^{-1} bar^{-1}) was calculated by the following equation (2):

$$P = J / \Delta P \tag{2}$$

where ΔP is the *trans*-membrane pressure loaded during nanofiltration experiments.

The rejection properties of the TFC membranes were tested by using a series of dyes dissolved in MeOH at a concentration of approximately 20 ppm. The absorbance spectra of the feeds and permeates were recorded via UV–vis spectrometer. Three consecutive permeates were collected and analyzed. Typically, results reported here were the average values of three tests. Equation (3) was used to calculate rejection (R):

$$R = \left(1 - \frac{C_p}{C_f}\right) \times 100\% \tag{3}$$

where C_p is the dye concentration of permeates and C_f is of feed solution.

3. Results and discussion

3.1. Characterizations of PA-AdDA nanofilms and PA-AdDA TFC membranes

The interfacial polymerization of AdDA in water and TMC *n*-hexane was employed to form PA-AdDA nanofilm, where the introduction of the adamantane group with a diamond-like cage structure in the resulting polyamide layer could effectively inhibit the chain packing, as schematically shown in Fig. 1a. A free-standing ultrathin PA-AdDA nanofilm could be formed on water/*n*-hexane interface. The PA-AdDA nanofilm is rather strong without any identifiable cracks after the action of external force (Fig. 1b and c). Different from the polyamide nanofilm prepared from PIP monomer, the PA-AdDA nanofilm possesses a special 3D

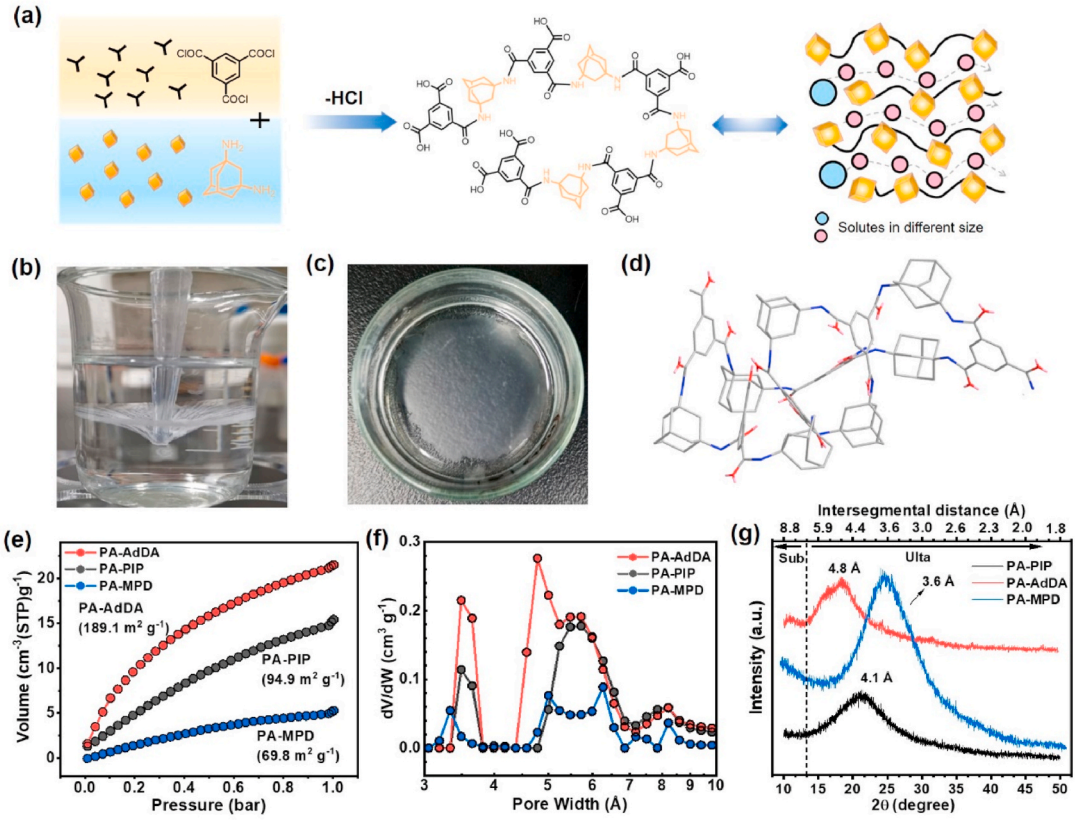

Fig. 1. Reaction and characterization of PA-AdDA nanofilm. (a) Schematic illustration of the reaction for preparation of PA-AdDA nanofilm using AdDA monomer. (b), (c) Digital photos of free-standing PA-AdDA nanofilm (d) three-dimensional model of PA-AdDA network. (e) CO_2 adsorption isotherms measured at 273 K, (f) pore size distributions, and (g) XRD patterns of PA-MPD nanofilm, PA-PIP and PA-AdDA nanofilms.

stereostructure endowed by the specific bulky cage-like geometry of adamantane (Fig. 1d). The surface area and pore size distribution of PA-AdDA nanofilm were probed by BET and XRD characterizations. The PA-MPD and PA-PIP nanofilms were also characterized for comparison. As shown in Fig. 1e, the BET surface area of PA-AdDA nanofilm is 189.1 m^2 g^{-1}, which is approximately 2–3 folds higher than that of PA-MPD nanofilm (69.8 m^2 g^{-1}) and PA-PIP nanofilm (94.9 m^2 g^{-1}). Pore size distributions of these nanofilms were calculated by non-local density functional theory (NLDFT) and the results are shown in Fig. 1f. All of nanofilms exhibit similar pore size distribution with ranges from 3.3 Å to 3.8 Å and 4.4 Å to 8.2 Å. The PA-AdDA nanofilm possesses more micropores as indicated by its higher fraction of micropore volume below 5 Å. The X-ray diffraction peaks in each pattern indicate the amorphous nature of these nanofilms [37]. Furthermore, the PA-AdDA nanofilm conceives the highest intersegmental distance (*d*-spacing) suggesting that the incorporation of adamantane structure can prevent the dense chain packing in the polymer and endow the nanofilm with higher free volume.

The PA-AdDA TFC membrane was directly fabricated on XP84 support and the morphology and thickness were characterized by SEM and AFM. As shown in Fig. 2a, regular cater-belt-like structures is observed on the membrane surface, with the concave parts of polyamide layer being surrounded by the protruding parts, which is different from the porous structure of the surface of XP84 support membrane (Fig. S1). Cross-sectional TEM image demonstrates that the thickness of the PA-AdDA selective layer of TFC membrane is around 50 nm (Fig. 2b) which is consist with that of the free-standing PA-AdDA nanofilm (Fig. 2c). Chemical structure of selective layer was discerned from ATR-FTIR and XPS spectra (Fig. 2d and e). The peaks at 1528 cm^{-1} and 1642 cm^{-1} are correlated to amide linkage N–H bending and the C═O stretching of polyamide [38]. The peak at 1722 cm^{-1} for C═O stretching of imide of XP84 support membrane was not observed. Meanwhile, $–CH_2$- stretching vibration which belongs to the AdDA building blocks can be seen at peaks of 2910 and 2855 cm^{-1} [39]. XPS analysis in Fig. 2 shows the chemical compositions of the PA-AdDA TFC membrane. The peak at 399.7 eV in N1s spectrum is assigned to amide bond (N–C═O) of polyamide. The peaks at O1s at 531.2 eV and 533.5 eV are attributed to the amide bond and carboxylic acid group (O–C═O) resulting from the hydrolysis of acyl chloride groups which indicates the successful fabrication of polyamide membrane [40]. The TGA measurement demonstrates that the PA-AdDA is thermally stable with decomposition temperature up to 400 °C in a nitrogen atmosphere (Fig. 2f), which is superior to that of conventional aromatic polyamides or polyesters with decomposition temperatures of ~ 300 °C [22,24]. The glass transition temperature of 109.4 °C is also observed for PA-AdDA via the DSC characterization (Inset Fig. 2f). The outstanding thermal stability of the as-prepared PA-AdDA is attributed to synergistic effects of highly crosslinked polyamide network with rigid adamantane building blocks

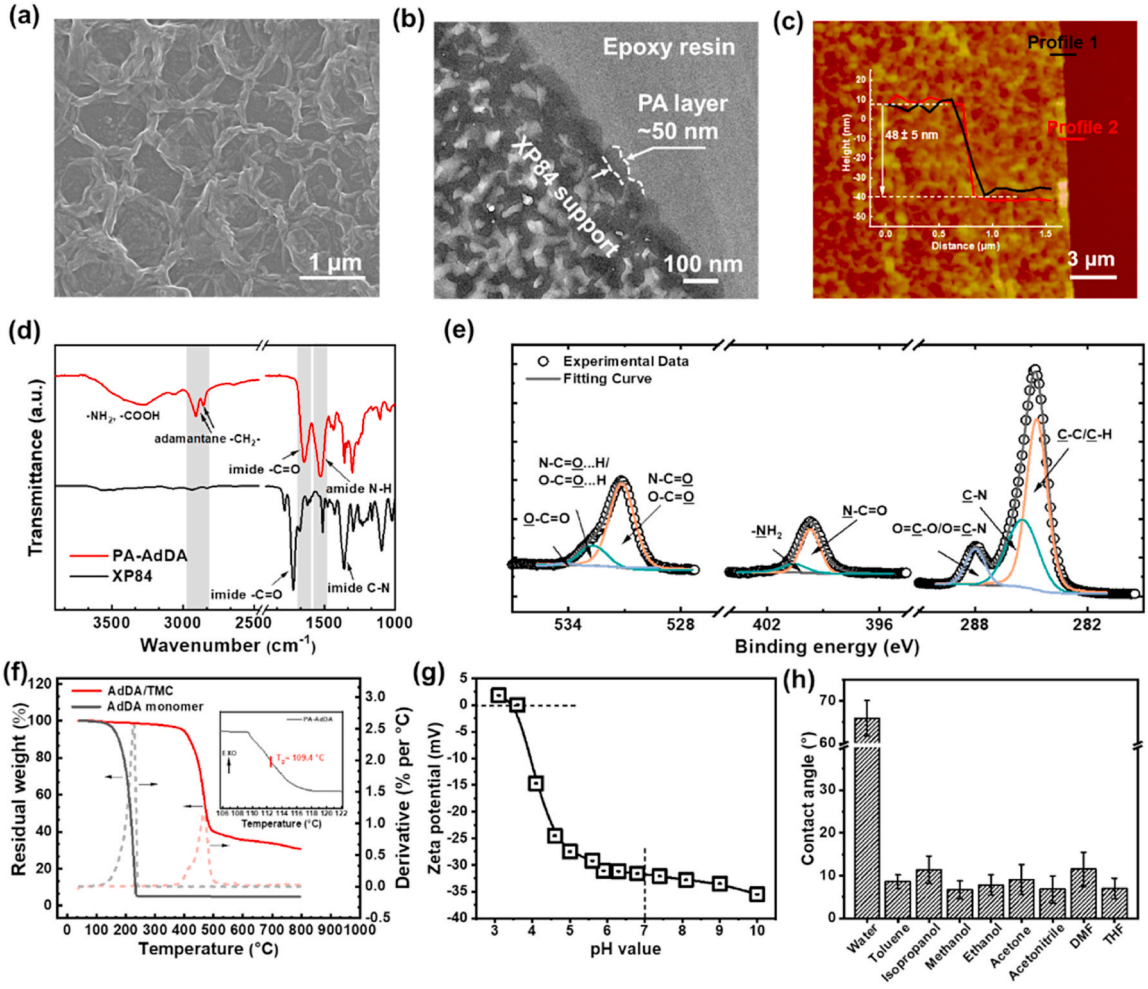

Fig. 2. Characterization of PA-AdDA TFC membrane. Taken the nanofilm and TFC membranes prepared by interfacial polymerization of diamines in aqueous solution (0.4 wt%) and TMC in *n*-hexane (0.32 wt%) with the reaction time of 10s as typical examples for the characterization. (a) SEM image of top surface of the membrane. (b) cross-sectional TEM image. (c) AFM image and corresponding height profiles of the selective layer. (d) ATR-FTIR and (e) XPS C 1s, N 1s and O 1s spectra of the PA-AdDA TFC membrane. (f) TGA and DSC (inset) profiles of PA-AdDA nanofilm. (g) Zeta potential of the PA-AdDA TFC membrane. (h) Surface wettability of the PA-AdDA TFC membrane to different solvents.

which stiffens the polymer chain and restricts the chain mobility. The surface charge of the PA-AdDA TFC membrane was investigated by measuring the solid surface zeta potentials over a pH range from 3 to 10. As shown in Fig. 2g, isoelectric point (IEP) of the membrane is pH = 3.6. At pH above the IEP, membrane displays negative charge due to the residual carboxylic acid groups on the membrane surface. The wettability measurements demonstrate that the PA-AdDA TFC membrane shows strong affinity for organic solvents both polar and nonpolar with contact angles of below 15° whereas poor affinity to water molecule with contact angle of above 65° due to the hydrophobicity of adamantly groups (Fig. 2h and Fig. S2). The strong affinity toward organic solvents is favor to the solvent dissolution into membrane and contributes to the transportation of solvents through the membranes.

3.2. OSN performance of PA-AdDA TFC membranes

The separation performance of PA-AdDA TFC membrane is primarily governed by the characteristics of selective layer. The selective layer was optimized via adjusting the reaction parameters including reactant concentration and reaction time as illustrated in Fig. 3. The effect of reactant concentration on selective layer of PA-AdDA membranes was evaluated by changing the concentration of AdDA concentration from 0.2 wt% to 0.8 wt% while the TMC concentration was fixed at 0.32 wt%. The detailed characterizations in terms morphology, thickness, surface charge and wettability of the membranes fabricated with different AdDA concentration was illustrated in Figs. S3–S5. The separation performances of the PA-AdDA TFC membranes were evaluated by measuring their permeance and dye rejection under the driving pressure of 10 bar, using MeOH solution containing MO as feed solution. Fig. 3a shows the variation in MeOH permeance and MO rejection as a function of AdDA concentration. The MeOH permeance decreases from 23.5 L m^{-2} h^{-1} bar^{-1} to 16.5 L m^{-2} h^{-1} bar^{-1} with increasing AdDA concentration from 0.2 wt% to 0.8 wt%, the decreased MeOH permeance may lie in the formation of thicker selective layer due to the longer monomer diffusion distance under higher AdDA concentration (Fig. S5) [41]. As for the rejection value of the PA-AdDA TFC membranes, the membrane fabricated at the lowest AdDA concentration of 0.2 wt% shows the MO rejection value of 60.3%. The rejection increases to 94.7% and 95.9% when increasing the AdDA concentration to 0.4 wt% and 0.6 wt%, respectively. However, the MO rejection decreases to 84.1% when further increasing AdDA concentration to 0.8 wt%. The compositions of the membranes are characterized by XPS analysis are illustrated in Figs. S6–S8 and Tables S2–S4. It is observed in O1s spectra that the content of -CONH- group increase with increasing AdDA concentration from 0.2 wt% to 0.6 wt%, further increasing the AdDA concentration to 0.8 wt% leads to the decrement of -CONH- groups. Whilst the content of $–NH_2$- groups increases with increasing AdDA concentration due to the unreacted amino groups during IP process [41]. The crosslinking degrees of the membranes obtained by XPS analysis are shown in Fig. 3b and Table S5. When AdDA concentration is 0.2 wt%, the crosslinking degree of the selective layer is 45.9%. The crosslinking degree increases to 72.7% and 83.7% when the AdDA concentration is 0.4 wt% and 0.6 wt%, respectively. Further increasing AdDA concentration to 0.8 wt%, the crosslinking degree of the selective layer decreases to 60.8%. These results are in accordance with the MO rejection value of the membranes. Fig. 3d illustrates the possible mechanism of the effect of AdDA concentration on the separation performance of the membranes. It is acknowledged that the concentration gradient between two immiscible phases determines the rate of monomer diffusion into the reaction zone. When the AdDA concentration is low in comparison with the TMC concentration of 0.32 wt%, the diffusion rate of AdDA molecules into the reaction zone is comparatively slow. Concentration mismatch between two monomers at the reaction zone makes the formation of a uniformly interconnected polyamide layer difficult. Reactions between two monomers generate primarily TMC-terminated complexes and then grows to form a loosely interconnected selective layer [42]. Likewise, when the AdDA concentration is much higher to than TMC concentration, similar loose selective layer with mostly AdDA-terminated complexes is obtained which results in lower MO rejection value. The influence of reaction time on the membrane performance was also evaluated. The PA-AdDA TFC membrane fabricated using the AdDA concentration of 0.4 wt% and TMC concentration of 0.32 wt% was chosen as a typical example, the results are depicted in Fig. 3c. By increasing the reaction time from 10 s to 60 s, MeOH permeance of the membranes decrease from 20.6 L m^{-2} h^{-1} bar^{-1} to 13.1 L m^{-2} h^{-1} bar^{-1} due to the increment of thickness of selective layer from 50 to 119 nm as shown in Fig. S9, whereas the MO rejection value

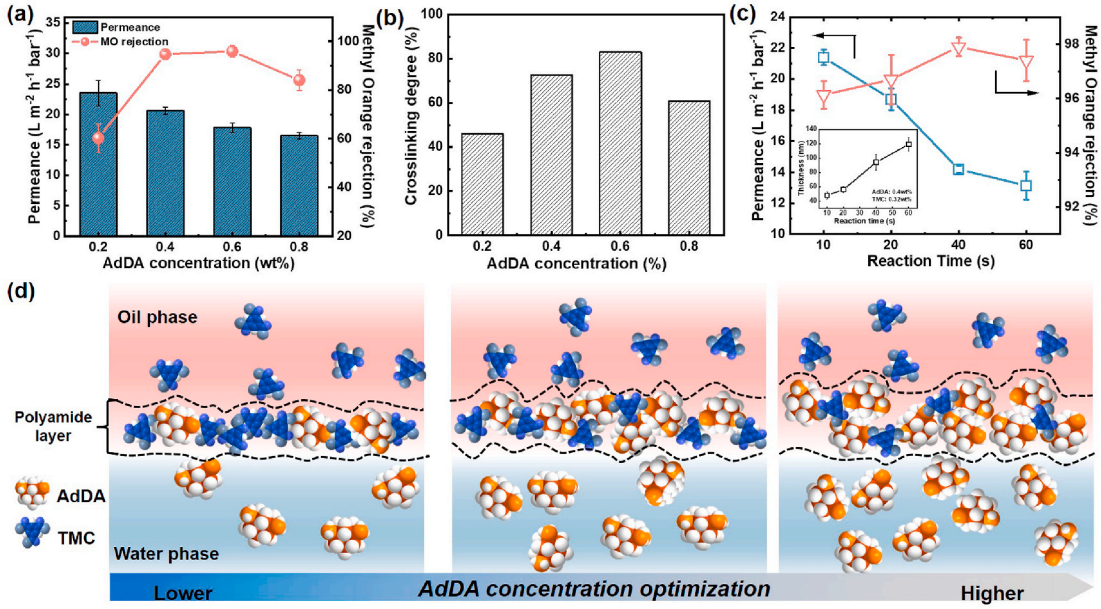

Fig. 3. Effects of AdDA concentration and reaction time on the performance of PA-AdDA TFC membranes. (a) MeOH permeance, MO rejection and (b) crosslinking degree of PA-AdDA TFC membranes with different AdDA concentrations. (c) MeOH permeance and MO rejection variation of PA-AdDA TFC membranes with different reaction time. Inset shows the variation of TFC membrane thickness at different reaction time. (d) Schematic illustration of the variations of selective layer fabricated from different AdDA concentrations.

remains nearly 95% without further increment. These results demonstrate the readily film-forming property of AdDA monomers thus building a dense selective layer within a short reaction time of 10s. The separation performance evaluation was conducted on the PA-AdDA TFC membrane fabricated at reaction time of 10s by monitoring the dye rejection of the membrane. Six dyes including MO, RhB, AF, CR, BBG250, BR with molecular weight ranging from 327.3 to 1017.6 g mol^{-1} were selected for the evaluation. The molecular weights, charges, sizes of the dye molecules are listed in Table S6. The dyes were dissolved in MeOH to form solutions with concentration of 20 ppm. The dye rejection values of the membranes are obtained by measuring the UV–vis absorption spectra of the feeds and permeates (Fig. S8), the dye concentrations are calculated based on their characteristic absorption peaks. As shown in Fig. 4a, the PA-AdDA TFC membrane demonstrates a clear removal of dyes with molecular weights higher than 327 g mol^{-1} showing high rejection value of ~ 95%, while their permeance are from 18.8 to 20.6 L m^{-2} h^{-1} bar^{-1}. The dye rejection decreases to 51.5% when filtrating CSG with lower molecular weight of 248.7 g mol^{-1} (Fig. S11). While the PA-MPD TFC membrane shows the permeance of 9.8 L m^{-2} h^{-1} bar^{-1} with similar rejection value to the selected dyes (Fig. S13). The molecular weight cut-off (MWCO) is defined as the molecular weight of the reference solute satisfying the membrane rejection rate of 90% and calculated from the MWCO curve featuring the dye rejection [43]. The MWCO of the PA-AdDA TFC membrane is 320 Da which is lower than that of PIMs membranes (500–800 Da), demonstrating its attractive separation performance for small solutes (Fig. S11). Slightly higher rejections of RhB, AF, BBG250 and BR can be attributed to their higher kinetic diameters and the molecular size rejected by the membrane, suggesting the size-based selectivity across the membrane. The rejection of neutral molecules in aqueous solution was also measured for the PA-AdDA TFC membrane. The MWCO of 235 Da with the mean pore size of 0.52 nm are smaller than those determined in methanol which may be due to the hydration effect of sugar molecules in aqueous solution. (Fig. S12). The mixed dye separation performance was conducted to evaluate the molecular sieving capability of the PA-AdDA TFC membrane, using CSG (Mw = 248.7 g mol^{-1}) and AF (Mw = 585.5 g mol^{-1}) mixture in MeOH, as schematically illustrated in Fig. 4b. As seen in the inset of Fig. 4c, the CSG and AF mixture is in color of vermilion, the permeate is in light yellow and retentate is rose red. This visual observation is further confirmed through UV–vis analysis (Fig. 4c). The UV–vis spectrum of the feed solution contains two characteristic absorption peaks at 444 nm and 552 nm corresponding to CSG and AF respectively, whereas only the absorption peak of CSG can be observed in permeate, suggesting that AF molecules are rejected by the PA-AdDA TFC membrane while allowing CSG molecules to pass through. The solvent transport behavior in PA-AdDA TFC membrane was characterized by investigating the permeation of several organic solvents, as depicted in Fig. 4d. A linear fit (R^2 = 0.94) is obtained between permeance and a combination of solvent physical parameter ($\delta_p\ \eta^{-1}\ d_m^{-2}$). δ_p, η and d_m stand for Hansen solubility parameter due to dipole forces, viscosity and molecular diameter of solvent, respectively. Solvent with low viscosity, small diameter and strong affinity to membrane gives high value of permeance. For example, acetonitrile, with the highest solubility parameter for polarity, relatively low viscosity and small molecular diameter (Table S7), shows high permeance of 28.0 L m^{-2} h^{-1} bar^{-1}. While the permeance value for toluene it is 0.34 L m^{-2} h^{-1} bar^{-1} due to the lowest value of $\delta_p\ \eta^{-1}\ d_m^{-2}$. The relationship between permeance and solvent physical parameters of PA-AdDA TFC membrane is in accordance with that of traditional polyamide membranes, suggesting that solvent transport across membrane is dominated by solution-diffusion theory. That is to say, solvents first dissolve into membrane surface then diffusing through the membrane during the transport process [8, 44]. Mass transfer process across the membrane is limited by the solubility and diffusivity of solvents, which makes δ_p, η and d_m non-negligible effect on membrane permeance. Fig. 4e and f provides a comparison of permselective performance of PA-AdDA TFC membrane and several state-of-the-art membranes from literatures, the detailed information is shown in Tables S8–S9. It can be seen that the permeance of the PA-AdDA TFC membrane is superior to that of most of the recently reported OSN membranes including conjugated microporous polymers (CMPs) membranes, polyester-CD et al., while the membrane exhibits good selectivity for organic solutes with lower MWCO of 320 Da, except for the sub-10 nm polyamide nanofilms (Fig. 4e). Fig. 4f shows a comparison of the permselectivity of membranes toward selected dye molecules including MO and RB. The results demonstrate that the PA-AdDA TFC membrane enhances permeance and dye rejection simultaneously

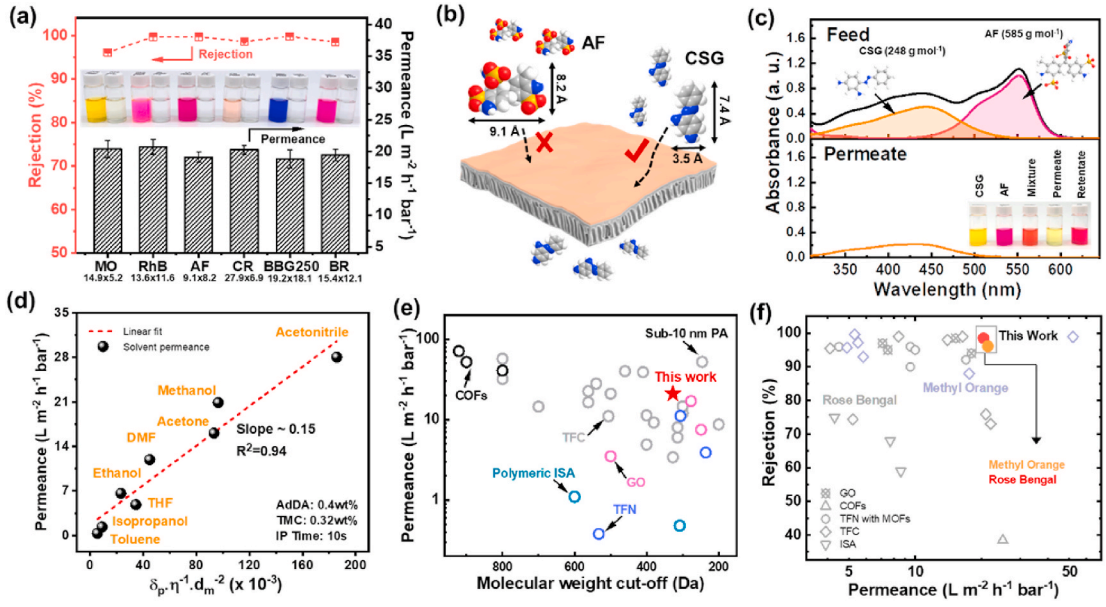

Fig. 4. Organic solvent nanofiltration performances of PA-AdDA TFC membrane. (a) Permeance and rejection of various dye solutions. Inset are the digital photos of feed and permeate solutions. (b) Schematic of the molecular sieving process. (c) UV spectra of the mixed dyes before and after filtration. Inset shows the optical photographs of feed, permeate and retentate solution. (d) Solvent permeance of the membrane versus combined solvent property. (e–f) Permselectivity comparison between the PA-AdDA TFC membrane with the state-of-the-art OSN membranes reported in literatures.

due to introduction of bulky cage-like adamantane structure in the membrane, which outperforms most of the reported membrane. The high permeance and the low MWCO give the potential to PA-AdDA TFC membrane in future OSN applications.

3.3. Operation stability of PA-AdDA TFC membranes

The pressure-resistance performance was evaluated by measuring the MeOH permeance and MO rejection under pressures ranging from 5 to 25 bar. As depicted in Fig. 5a, solvent flux increases linearly with increasing applied pressure while the rejection rate of MO remains at around 95%, suggesting that the microporous structures formed inside membrane are stable under compression. The solvent stability for PA-AdDA TFC membrane was investigated by ordinal filtration of solvents MeOH, acetone, THF and toluene through the membrane, the MeOH was filtrated through the membrane again. The filtration time of each solvent is 3 h and the permeance of the membrane was monitored during the filtration. The MeOH permeance slightly decreases from 21.3 to 19.7 L m^{-2} h^{-1} bar^{-1} with decline ratio of ~7.5% after filtration of different solvents showing good stability of membrane. The long-term stability of PA-AdDA TFC membrane was characterized by continuous filtration the MO solutions in various solvents of different polarities including DMF, MeOH and *n*-hexane for 180 h at 10 bar, the concentration of the solutions are 20 ppm. The membranes were compacted for at least 6 h at 10 bar before permeance measurement until the permeate flux was stable. As shown in Fig. 5c, the membrane keeps stable permeance of approximately ~20.1 L m^{-2} h^{-1} bar^{-1} for MeOH, ~12.3 L m^{-2} h^{-1} bar^{-1} for DMF, and ~ 2.1 L m^{-2} h^{-1} bar^{-1} for *n*-hexane during180 h continuous filtration. The separation performance of the PA-AdDA TFC membrane during the long-term test was also evaluated using the DMF solution containing MO as a typical example. As shown in Fig. 5d, the MO rejection in DMF maintains around 94% over 180 h filtration. Digital photos of PA-AdDA TFC membrane before and after long-term separation are shown in the inset of Fig. 5d. Visually, no obvious membrane swelling can be observed in the testing area with a diameter of 2 cm. The SEM images in Fig. S14 shows that the surface morphology of the membrane becomes blurred after long-term test in DMF solution, which might be ascribed to the membrane compaction at high pressure.

4. Conclusion

In summary, PA-AdDA TFC membrane with high permeance over polar solvents and low MWCO of 320 Da was fabricated by interfacial polymerization using AdDA as monomer in aqueous phase. The AdDA monomer, featuring rigid and bulky structures, takes the role of steric hindrance unit to increase microporosity within the selective layer. The PA-AdDA TFC membrane achieves improved solvent permeances without sacrificing the selectivity toward dyes, and it also possesses stable separation performance in various organic solutions. The PA-AdDA TFC membrane exhibits a MeOH permeance of up to 20.6 L m^{-2} h^{-1} bar^{-1} and a MO rejection of up to 94.7%, which outperforms most of the state-of-the-art membranes. This work provides some insights to the development of high-performance TFC OSN membranes through structural regulation of monomers.

Author statement

Siyan Wang, Feng Zhang and Jian Jin designed the experiments. Siyan Wang, Shouwen Zhu and Shuqi Liu conducted the experiments and material characterizations. Zhenggong Wang, Feng Zhang and Jian Jin provided helpful discussion. Siyan Wang, Feng Zhang and Jian Jin wrote the manuscript. All of the authors participated in the discussion and read the manuscript.

Declaration of competing interest

The authors declare that they have no known competing financial interests or personal relationships that could have appeared to influence the work reported in this paper.

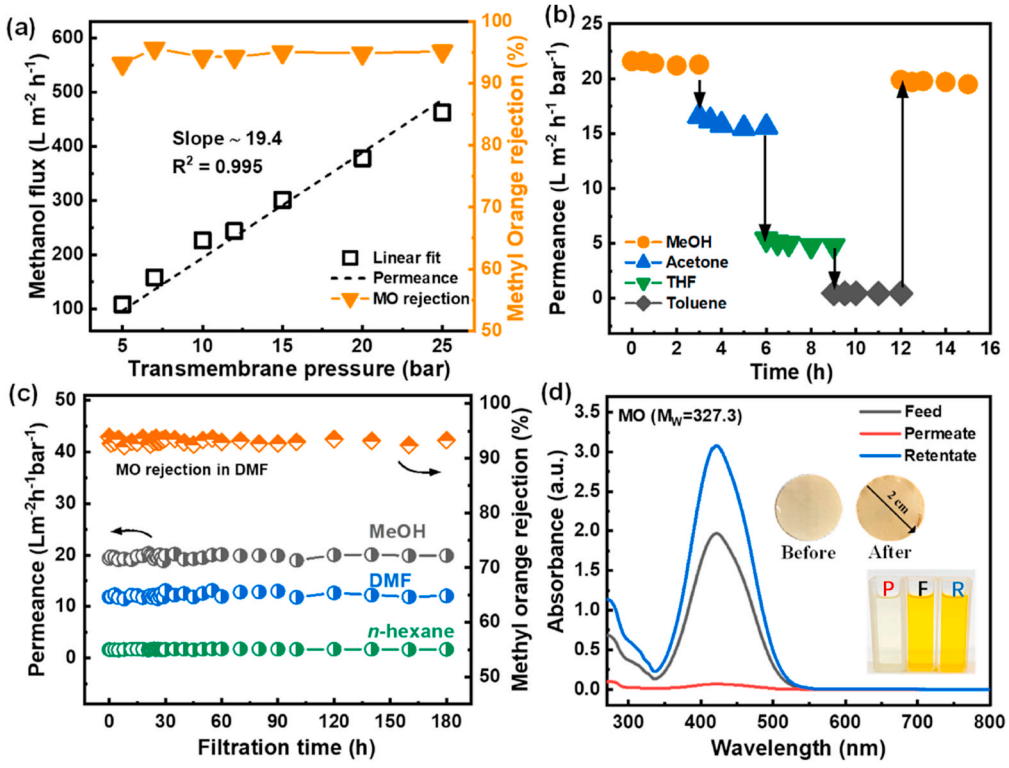

Fig. 5. Stability of the PA-AdDA TFC membranes. (a) Pressure-resistance test of the membrane evaluated in the pressure range from 5 to 25 bar. (b) Solvent-resistance test evaluated by solvents with different polarities. (c) Long-term operation test of the PA-AdDA TFC membranes in solvents of MeOH, *n*-hexane and aggressive DMF for 180 h. (d) UV absorption spectra and digital photos of the feed, permeate and retentate, inset are digital photos of PA-AdDA TFC membrane before and after long-term test.

Data availability

No data was used for the research described in the article.

Acknowledgment

The authors thank the financial support from National Key Research and Development Plan (2022YFB3805903, 2019YFA0705800), National Natural Science Foundation of China (21988102), and the Key Development Project of Jiangsu Province (BE2022056).

Appendix A. Supplementary data

Supplementary data to this article can be found online at https://doi.org/10.1016/j.memsci.2023.121540.

References

[1] D. Ren, S. Ren, Y. Lin, J. Xu, X. Wang, Recent developments of organic solvent resistant materials for membrane separations, Chemosphere 271 (2021), 129425, https://doi.org/10.1016/j.chemosphere.2020.129425.
[2] P. Marchetti, M.F. Jimenez Solomon, G. Szekely, A.G. Livingston, Molecular separation with organic solvent nanofiltration: a critical review, Chem. Rev. 114 (2014) 10735–10806, https://doi.org/10.1021/cr500006j.
[3] Y. Li, Z. Guo, S. Li, B. Van der Bruggen, Interfacially polymerized thin-film composite membranes for organic solvent nanofiltration, Adv. Mater. Interfac. 8 (2021), 2001671, https://doi.org/10.1002/admi.202001671.
[4] Y. Xu, J. Lin, C. Gao, B. Van der Bruggen, Q. Shen, H. Shao, J. Shen, Preparation of high-flux nanoporous solvent resistant polyacrylonitrile membrane with potential fractionation of Dyes and Na_2SO_4, Ind. Eng. Chem. Res. 56 (2017) 11967–11976, https://doi.org/10.1021/acs.iecr.7b03409.
[5] S. Karan, Z. Jiang, A.G. Livingston, Sub-10 nm polyamide nanofilms with ultrafast solvent transport for molecular separation, Science 348 (2015) 1347–1351, https://doi.org/10.1126/science.aaa5058.
[6] G.M. Shi, Y. Feng, B. Li, H.M. Tham, J.-Y. Lai, T.-S. Chung, Recent progress of organic solvent nanofiltration membranes, Prog. Polym. Sci. 123 (2021), 101470, https://doi.org/10.1016/j.progpolymsci.2021.101470.
[7] H. Wang, M. Wang, X. Liang, J. Yuan, H. Yang, S. Wang, Y. Ren, H. Wu, F. Pan, Z. Jiang, Organic molecular sieve membranes for chemical separations, Chem. Soc. Rev. 50 (2021) 5468–5516, https://doi.org/10.1039/d0cs01347a.
[8] D.B. Shinde, G. Sheng, X. Li, M. Ostwal, A.H. Emwas, K.W. Huang, Z. Lai, Crystalline 2D covalent organic framework membranes for high-flux organic solvent nanofiltration, J. Am. Chem. Soc. 140 (2018) 14342–14349, https://doi.org/10.1021/jacs.8b08788.
[9] K. Dey, M. Pal, K.C. Rout, H.S. Kunjattu, A. Das, R. Mukherjee, U.K. Kharul, R. Banerjee, Selective molecular separation by interfacially crystallized covalent organic framework thin films, J. Am. Chem. Soc. 139 (2017) 13083–13091, https://doi.org/10.1021/jacs.7b06640.
[10] Y. Li, Q. Wu, X. Guo, M. Zhang, B. Chen, G. Wei, X. Li, X. Li, S. Li, L. Ma, Laminated self-standing covalent organic framework membrane with uniformly distributed subnanopores for ionic and molecular sieving, Nat. Commun. 11 (2020) 599, https://doi.org/10.1038/s41467-019-14056-7.
[11] S. Kandambeth, B.P. Biswal, H.D. Chaudhari, K.C. Rout, H.S. Kunjattu, S. Mitra, S. Karak, A. Das, R. Mukherjee, U.K. Kharul, R. Banerjee, Selective molecular sieving in self-standing porous covalent-organic-framework membranes, Adv. Mater. 29 (2017), 1603945, https://doi.org/10.1002/adma.201603945.
[12] S. Sorribas, P. Gorgojo, C. Tellez, J. Coronas, A.G. Livingston, High flux thin film nanocomposite membranes based on metal-organic frameworks for organic solvent nanofiltration, J. Am. Chem. Soc. 135 (2013) 15201–15208, https://doi.org/10.1021/ja407665w.
[13] A. Asadi Tashvigh, N.E. Benes, Covalent organic polymers for aqueous and organic solvent nanofiltration, Separ. Purif. Technol. 298 (2022), 121589, https://doi.org/10.1016/j.seppur.2022.121589.
[14] Z. Tan, S. Chen, X. Peng, Z. Lin, G. Congjie, Polyamide membranes with nanoscale turing structures for water purification, Science 360 (2018) 518–521.
[15] Y. Liang, Y. Zhu, C. Liu, K.-R. Lee, W.-S. Hung, Z. Wang, Y. Li, M. Elimelech, J. Jin, S. Lin, Polyamide nanofiltration membrane with highly uniform sub-nanometre pores for sub-1 angstrom precision separation, Nat. Commun. 11 (2020) (2015), https://doi.org/10.1038/s41467-020-15771-2.
[16] D. Ren, Y.H. Li, S.P. Ren, T.Y. Liu, X.L. Wang, Microporous polyarylate membrane with nitrogen-containing heterocycles to enhance separation performance for organic solvent nanofiltration, J. Membr. Sci. 610 (2020), 118295, https://doi.org/10.1016/j.memsci.2020.118295.
[17] T. Huang, T. Puspasari, S.P. Nunes, K.V. Peinemann, Ultrathin 2D-layered cyclodextrin membranes for high-performance organic solvent nanofiltration, Adv. Funct. Mater. 30 (2019), 1906797, https://doi.org/10.1002/adfm.201906797.
[18] S.L. Li, G. Chang, Y. Huang, K. Kinooka, Y. Chen, W. Fu, G. Gong, T. Yoshioka, N. B. McKeown, Y. Hu, 2,2'-Biphenol-based ultrathin microporous nanofilms for highly efficient molecular sieving separation, Angew. Chem. Int. Ed. 61 (2022), e202212816, https://doi.org/10.1002/anie.202212816.
[19] A. Asadi Tashvigh, M.G. Elshof, N.E. Benes, Development of thin-film composite membranes for nanofiltration at extreme pH, ACS Applied Polymer Materials 3 (2021) 5912–5919, https://doi.org/10.1021/acsapm.1c01172.
[20] N.B. McKeown, Polymers of intrinsic microporosity (PIMs), Polymer 202 (2020), 122736, https://doi.org/10.1016/j.polymer.2020.122736.
[21] M.A. Abdulhamid, G. Szekely, Organic solvent nanofiltration membranes based on polymers of intrinsic microporosity, Curr. Opin.Chem. Eng 36 (2022), 100804, https://doi.org/10.1016/j.coche.2022.100804.
[22] M.F. Jimenez-Solomon, Q. Song, K.E. Jelfs, M. Munoz-Ibanez, A.G. Livingston, Polymer nanofilms with enhanced microporosity by interfacial polymerization, Nat. Mater. 15 (2016) 760–767, https://doi.org/10.1038/nmat4638.
[23] C. Jiang, L. Tian, Y. Hou, Q.J. Niu, Nanofiltration membranes with enhanced microporosity and inner-pore interconnectivity for water treatment: excellent balance between permeability and selectivity, J. Membr. Sci. 586 (2019) 192–201, https://doi.org/10.1016/j.memsci.2019.05.075.
[24] Z. Ali, B.S. Ghanem, Y. Wang, F. Pacheco, W. Ogieglo, H. Vovusha, G. Genduso, U. Schwingenschlogl, Y. Han, I. Pinnau, Finely tuned submicroporous thin-film molecular sieve membranes for highly efficient fluid separations, Adv. Mater. 32 (2020), 2001132, https://doi.org/10.1002/adma.202001132.
[25] X. Ma, I. Pinnau, Effect of film thickness and physical aging on "intrinsic" gas permeation properties of microporous ethanoanthracene-based polyimides, Macromolecules 51 (2018) 1069–1076, https://doi.org/10.1021/acs.macromol.7b02556.
[26] A. Asadi Tashvigh, T.-S. Chung, Robust polybenzimidazole (PBI) hollow fiber membranes for organic solvent nanofiltration, J. Membr. Sci. 572 (2019) 580–587, https://doi.org/10.1016/j.memsci.2018.11.048.
[27] S.J. Xu, L.H. Luo, Y.H. Tong, Q. Shen, Z.-L. Xu, Y.-Z. Wu, H. Yang, Organic solvent nanofiltration (OSN) membrane with polyamantadinamide active layer for reducing separation performance inconformity, Separ. Purif. Technol. 278 (2021), 119582, https://doi.org/10.1016/j.seppur.2021.119582.
[28] C. Aguilar-Lugo, C. Álvarez, Y.M. Lee, J.G. de la Campa, Á.E. Lozano, Thermally rearranged polybenzoxazoles containing bulky adamantyl groups from ortho-substituted precursor copolyimides, Macromolecules 51 (2018) 1605–1619, https://doi.org/10.1021/acs.macromol.7b02460.
[29] B. Shrimant, S.V. Shaligram, U.K. Kharul, P.P. Wadgaonkar, Synthesis, characterization, and gas permeation properties of adamantane-containing polymers of intrinsic microporosity, J. Polym. Sci. Polym. Chem. 56 (2018) 16–24, https://doi.org/10.1002/pola.28710.
[30] Z. Wang, Q. Shen, J. Liang, Y. Zhang, J. Jin, Adamantane-grafted polymer of intrinsic microporosity with finely tuned interchain spacing for improved CO_2 separation performance, Separ. Purif. Technol. 233 (2020), 116008, https://doi.org/10.1016/j.seppur.2019.116008.
[31] E.M. Maya, I. García-Yoldi, A.E. Lozano, J.G. de la Campa, J. de Abajo, Synthesis, characterization, and gas separation properties of novel copolyimides containing adamantyl ester pendant groups, Macromolecules 44 (2011) 2780–2790, https://doi.org/10.1021/ma200093j.
[32] M.R. Pixton, D.R. Paul, Gas transport properties of adamantane-based polysulfones, Polymer 36 (1995) 3165–3172, https://doi.org/10.1016/0032-3861(95)97880-O.
[33] E.J. Kappert, M.J.T. Raaijmakers, K. Tempelman, F.P. Cuperus, W. Ogieglo, N. E. Benes, Swelling of 9 polymers commonly employed for solvent-resistant nanofiltration membranes: a comprehensive dataset, J. Membr. Sci. 569 (2019) 177–199, https://doi.org/10.1016/j.memsci.2018.09.059.
[34] G.M. Shi, Y. Feng, B. Li, H.M. Tham, J.Y. Lai, T.S. Chung, Recent progress of organic solvent nanofiltration membranes, Prog. Polym. Sci. 123 (2021), 101470, https://doi.org/10.1016/j.progpolymsci.2021.101470.
[35] Y. Lu, R. Wang, Y. Zhu, Z. Wang, W. Fang, S. Lin, J. Jin, Two-dimensional fractal nanocrystals templating for substantial performance enhancement of polyamide nanofiltration membrane, Proc. Natl. Acad. Sci. USA 118 (2021), e2019891118, https://doi.org/10.1073/pnas.2019891118.
[36] Z. Wang, Z. Wang, S. Lin, H. Jin, S. Gao, Y. Zhu, J. Jin, Nanoparticle-templated nanofiltration membranes for ultrahigh performance desalination, Nat. Commun. 9 (2018) (2004), https://doi.org/10.1038/s41467-018-04467-3.
[37] X. Shui, J. Li, M. Zhang, C. Fang, L. Zhu, Tailoring ultrathin microporous polyamide films with rapid solvent transport by molecular layer-by-layer deposition, J. Membr. Sci. 628 (2021), 119249, https://doi.org/10.1016/j.memsci.2021.119249.
[38] S. Li, R. Zhang, Q. Yao, B. Su, L. Han, C. Gao, High flux thin film composite (TFC) membrane with non-planar rigid twisted structures for organic solvent nanofiltration (OSN), Separ. Purif. Technol. 286 (2022), 120496, https://doi.org/10.1016/j.seppur.2022.120496.
[39] S.J. Xu, Q. Shen, Z.L. Xu, Z.Q. Dong, Novel designed TFC membrane based on host-guest interaction for organic solvent nanofiltration (OSN), J. Membr. Sci. 588 (2019), 117227, https://doi.org/10.1016/j.memsci.2019.117227.
[40] T. Huang, B.A. Moosa, P. Hoang, J. Liu, S. Chisca, G. Zhang, M. AlYami, N. M. Khashab, S.P. Nunes, Molecularly-porous ultrathin membranes for highly selective organic solvent nanofiltration, Nat. Commun. 11 (2020) 5882, https://doi.org/10.1038/s41467-020-19404-6.
[41] J. Tian, H. Chang, S. Gao, Y. Zong, B. Van der Bruggen, R. Zhang, Direct generation of an ultrathin (8.5 nm) polyamide film with ultrahigh water permeance via in-situ interfacial polymerization on commercial substrate membrane, J. Membr. Sci. 634 (2021), 119450, https://doi.org/10.1016/j.memsci.2021.119450.

[42] P. Sarkar, S. Modak, S. Karan, Ultraselective and highly permeable polyamide nanofilms for ionic and molecular nanofiltration, Adv. Funct. Mater. 31 (2020), 2007054, https://doi.org/10.1002/adfm.202007054.
[43] J. Jang, Y.T. Nam, D. Kim, Y.J. Kim, D.W. Kim, H.T. Jung, Turbostratic nanoporous carbon sheet membrane for ultrafast and selective nanofiltration in viscous green solvents, J. Mater. Chem. 8 (2020) 8292–8299, https://doi.org/10.1039/d0ta00804d.
[44] D. Paul, Reformulation of the solution-diffusion theory of reverse osmosis, J. Membr. Sci. 241 (2004) 371–386, https://doi.org/10.1016/j.memsci.2004.05.026.